Scholar Publishing Group
Kinetic Mechanical Engineering
https://doi.org/10.38007/KME.2023.040205
ISSN 2790-2676 Vol. 4, Issue 2: 38-47

# *Research on Macro-Micro Mechanical Properties of Cable Tower Surface Based on Multiscale Homogenization Theory*

**Fucai Pei[1] and Ranran Hu[2]**

[1]*Shandong Luqiao Group Co., Ltd., Shandong, China*

[2]*Shandong Jiaotong University, Shandong, China*

***Keywords:*** Cable-stayed Bridge, Non-homogeneous Materials, Microscopic Structures, Particle Flow

***Abstract:*** Cable-stayed Bridge got rapidly developed in designing and constructing during these decades. Concrete cable-stayed bridge [1-6] occupies larger proportion. Tall cable towers' cracking behavior has aroused more and more attention from the researchers. Under the outer load, temperature load, concrete shrinkage and creep effect, tower of concrete cable-stayed bridge suffers huge pressure transmitted by cables. According to incomplete statistics, tower fracture occurs in 80% of the Chinese cable bridges, it seriously affects the cable-stayed bridge's safety and even people's life. This article introduced the fractal damage and the fractal fracture mechanics into safety assessment of cable-stayed bridge's cable tower. Then, tall tower' safety state evaluation model is put forward based on fracture distribution in this paper Beginning and expansion of fractures and the structure failure process are analyzed from the macroscopic and mesoscopic point of view through theoretical analysis. This paper set up a new method supported by the theory of fractal damage for evaluation of cable tower safety state after cracking occurs. The relationship between the load level and fractal dimension of fracture distribution after the cable tower cracking occurs is researched and it provides theoretical and experimental basis to further application to real bridge. The following mainly innovative work has been done in this paper.

## 1. Theoretical Basis

Homogenization theory is an effective multiscale computing method that takes unit cells as the basic research object. And unit cells constitute the microscopic and mesoscopic structure of materials. Assuming that unit cells have space repeatability, that is assuming that the microstructure

Copyright: © 2023 by the authors. This is an Open Access article distributed under the Creative Commons Attribution License (CC BY 4.0), which permits unrestricted use, distribution, and reproduction in any medium, provided the original work is properly cited (https://creativecommons.org/licenses/by/4.0/).

is periodic or quasi-periodic, by introducing macroscopic and microscopic scales and considering the mechanical behavior of the material's macroscopic and microscopic structures, the equivalence relationships between macroscopic and microscopic structures can be bridged. Technology Roadmapis shown in Figure 2.The theory adopts the form of perturbation solutions, expanding physical quantities such as displacement and stress at a point in the macroscopic structure into asymptotic series of perturbation which is related to microstructural scale. Then it use the principle of virtual work (or variational principle) to get the unit cell equation and introducing the equation to the unit load and boundary conditions, the macroscopic mechanical properties of the material can be effectively predicted, eventually the macroscopic mechanical properties of the material can be predicted.

Assuming there is a concrete material structure liking the figure 1, which occupies Ω in R3 space, the microstructural can be thought as a periodic repetition rank. of non-homogeneous unit cells in space at a macroscopic point. Presuming the object is subjected to a volumetric force f, a surface force on the force boundary Γt, and a given displacement on the displacement boundary Γv.

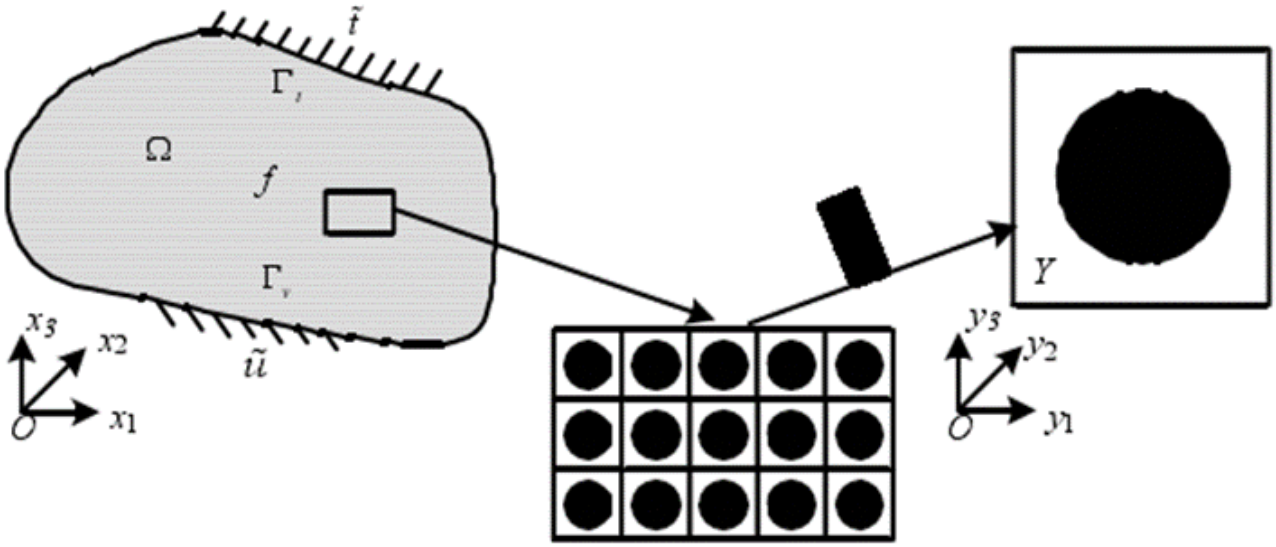


*Figure 1. Schematic diagram of periodic non-homogenous material and its unit cell*

For practical non-homogeneous materials, its high non-homogenization in microstructure will lead to the structural field variables such as displacement and stress to vary drastically within a certain neighborhood ε. To deal with such problems with macroscale and mesoscale, it is advisable to use a mesoscale y= x/ε. Where x is the macroscopic coordinate; y is the microscopic coordinate; and 1/ε is the amplification factor. For any point x in the macroscopic coordinates of the concrete structure, commanding its microstructure is periodic repetition rank, all functions related to the Mesoscopic coordinates are periodic. The size of the unit cell is relatively small compared to the macroscopic geometric scale, and is assumed to be of the order of ε ($0 \leqslant \varepsilon \leqslant 1$). By using the coordinate transformation y = x/ε, a point in Ω is magnified into a unit cell Y, and the equivalent elastic properties can be acknowledged.

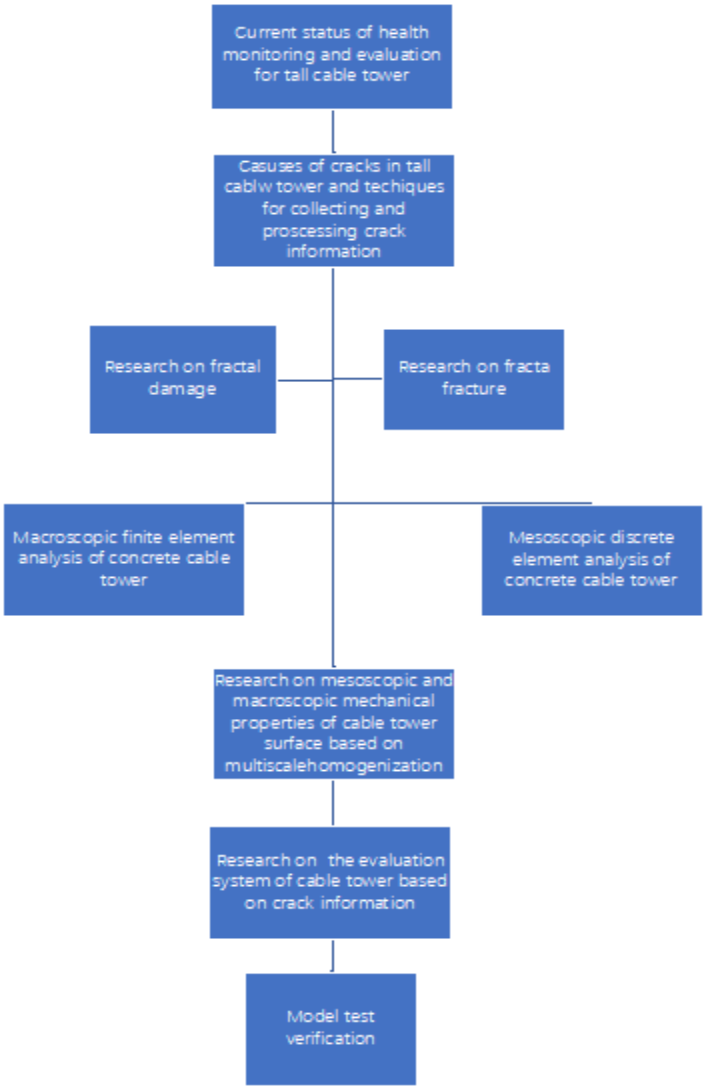


*Figure 2. Technology Roadmap*

Assuming the unit cell is a linear elastic medium, the following basic equations and boundary conditions are satisfied in $\Omega$:

Balance equation: $\sigma_{ij,j}^{\varepsilon} + f_i = 0$

Geometric equation: $e_{ij}^{\varepsilon} = \frac{1}{2}\left(u_{i,j}^{\varepsilon} + u_{j,i}^{\varepsilon}\right)$

Constitutive equation: $\sigma_{ij}^{\varepsilon} = E_{ijkl}^{\varepsilon} e_{kl}^{\varepsilon}$

Boundary conditions: $\sigma_{ij}^{\varepsilon} n_i = \tilde{\tau}_i$

Displacement conditions: $u_i^{\varepsilon} = \tilde{u}_i$

In the equations above, $E_{ijkl}^{\varepsilon}$ represents elastic tensor of the material, $u_i^{\varepsilon}$ represents displacement tensor, $\sigma_{ij}^{\varepsilon}$ represents stress tensor, $e_{ij}^{\varepsilon}$ represents strain tensor, $n$ represents the unit normal vector in the $\partial\Omega$ boundary, $\varepsilon$ as the superscript represents the characteristic of double scales of the function. Based on the technique that slowly expanding, the displacement of $u^{\varepsilon}(x)$ at any point on the $\Omega$ domain can be expressed as:

$$u^{\varepsilon}(x) = u^{0}(x,y) + \varepsilon u^{1}(x,y) + \varepsilon^{2} u^{2}(x,y) + \cdots \ldots \quad (1)$$

The terms expanded in equation (1) characterize the fine-scale oscillations of the displacement field. As the number of expansion terms increases, equation (1) gradually approaches the oscillatory behavior of the true displacement field at the micro-mesoscopic scale. Based on the principle of virtual displacement, it can be shown that:

$$\int_\Omega E_{ijkl}\frac{\partial u_k^\varepsilon}{\partial x_l}\frac{\partial v_i}{\partial x_j}d\Omega = \int f_i^\varepsilon v_i d\Omega + \int_{\Gamma_i}\tilde{t}_i v_i d\Gamma \tag{2}$$

Accordingly, $v_i$ represents the virtue displacement which satisfies the boundary conditions, $E_{ijkl}$ represents the elastic tensor of the material, The rest of the variables satisfies equation (3).

$$E_{ijkl} = E_{jikl} = E_{ijlk} = E_{klij} \tag{3}$$

bring the formula (2) into the formula (3):

$$\int_\Omega E_{ijkl}\frac{\partial v_i}{\partial x_j}\frac{\partial}{\partial x_l}(u_k^0 + \varepsilon u_k^1 + \varepsilon^2 u_k^2 + \cdots)d\Omega = \int_\Omega f_i^\varepsilon v_i d\Omega + \int_{\Gamma_i}\tilde{t}_i v_i d\Gamma \tag{4}$$

According to the characteristics of periodic functions, any Y-periodic function satisfies formula (5), additionally, $y$ is a variable dependent on $x$:

$$\frac{d\phi}{dx} = \frac{\partial\phi}{\partial x} + \frac{\partial\phi}{\partial y}\frac{\partial y}{\partial x} \tag{5}$$

If $y = x/\varepsilon$, formula (5) can be transferred to formula (6):

$$\frac{d\phi}{dx} = \frac{\partial\phi}{\partial x} + \frac{1}{\varepsilon}\frac{\partial\phi}{\partial y} \tag{6}$$

Formula (7) will be obtained after taking formula (6) into formula (4):

$$\begin{aligned}\int_\Omega E_{ijkl}\{&\frac{1}{\varepsilon^2}\frac{\partial u_k^0}{\partial y_l}\frac{\partial v_i}{\partial y_j} + \frac{1}{\varepsilon}[(\frac{\partial u_k^0}{\partial x_l} + \frac{\partial u_k^1}{\partial y_l})\frac{\partial v_i}{\partial y_j} + \frac{\partial u_k^0}{\partial y_l}\frac{\partial v_i}{\partial x_j}] + [(\frac{\partial u_k^0}{\partial x_l} + \frac{\partial u_k^1}{\partial y_l})\frac{\partial v_i}{\partial y_j}\\ &+(\frac{\partial u_k^1}{\partial x_l} + \frac{\partial u_k^2}{\partial y_l})\frac{\partial v_i}{\partial x_j}] + \varepsilon(\dots)\}d\Omega = \int_\Omega f_i^\varepsilon v_i d\Omega + \int_{\Gamma_i}\tilde{t}_i v_i d\Gamma\end{aligned} \tag{7}$$

According to the characteristic of periodic function, Y-periodic function $\phi(x)$ satisfies formula (8) below:

$$\lim_{\varepsilon\to 0^+}\int_\Omega \phi(\frac{x}{\varepsilon})d\Omega = \frac{1}{|Y|}\int_\Omega\int_Y \phi(y)dYd\Omega \tag{8}$$

Substituting equation (8) into equation (7) and setting the coefficients of each power to zero simultaneously, a differential equation relating $u^0$ $u^1$ and $u^2$ can be shown below:

$$\frac{1}{|Y|}\int_\Omega\int_Y E_{ijkl}\frac{\partial u_k^0}{\partial y_l}\frac{\partial v_i}{\partial y_j}dYd\Omega = 0 \tag{9}$$

$$\frac{1}{|Y|}\int_\Omega\int_Y E_{ijkl}[(\frac{\partial u_k^0}{\partial x_l} + \frac{\partial u_k^1}{\partial y_l})\frac{\partial v_i}{\partial y_j} + \frac{\partial u_k^0}{\partial y_l}\frac{\partial v_i}{\partial x_j}]dYd\Omega = 0 \tag{10}$$

$$\begin{aligned}\frac{1}{|Y|}\int_\Omega\int_Y E_{ijkl}[&(\frac{\partial u_k^1}{\partial x_l} + \frac{\partial u_k^2}{\partial y_l})\frac{\partial v_i}{\partial y_j} + (\frac{\partial u_k^0}{\partial x_l} + \frac{\partial u_k^1}{\partial y_l})\frac{\partial v_i}{\partial x_j}]dYd\Omega\\ &= \int_\Omega(\frac{1}{|Y|}\int_Y f_i v_i dY)d\Omega + \int_{\Gamma_i}\tilde{t}_i v_i d\Gamma\end{aligned} \tag{11}$$

Since $v$ is an arbitrary function, it is advisable to chooze $v = v(y)$ and then integrate it step by step, after applying the non-homogenization theory and its periodicity on the integration domain Y, equation (12) appears:

$$\frac{1}{|Y|}\int_{\Omega}\{\int_{Y}[-\frac{\partial}{\partial y_i}(E_{ijkl}\frac{\partial u_k^0}{\partial y_l})]v_i dY+\int_{s}E_{ijkl}\frac{\partial u_k^0}{\partial y_l}n_j v_i ds\}d\Omega=0 \quad (12)$$

Because v is arbitrary, so:

$$-\frac{\partial}{\partial y_i}(E_{ijkl}\frac{\partial u_k^0}{\partial y_l})=0, \quad \forall y\in Y \quad (13)$$

$$E_{ijkl}\frac{\partial u_k^0}{\partial y_l}n_j=0, \quad (14)$$

Considering the characteristic of Y-periodic function and equation (12), there is equation (15) below:

$$u^0(x,y)=u^0(x) \quad (15)$$

That is, the first term of the asymptotic expansion is only related to the macroscopic coordinates.

## 2. The Influence of Cell Size on Concrete Properties

Concrete materials have a minimum period [7-10] , when the unit cell size is less than this period, The results cannot fully reflect the mechanical characteristics of concrete; when it is greater than this period, the results obtained tend to stable, but it will increase the amount of numerical calculation and storage. Therefore, it is necessary to first find a suitable unit cell size to test its impact to concrete properties. The discrete element method is used to generate 20 groups of concrete models with different cell sizes and particle sizes ranging from 5 to 10 mm, with each group containing five samples with different aggregate distributions. A cell sample with a size of 30 mm ×30 mm is used as an example to establish a discrete element concrete cell model.

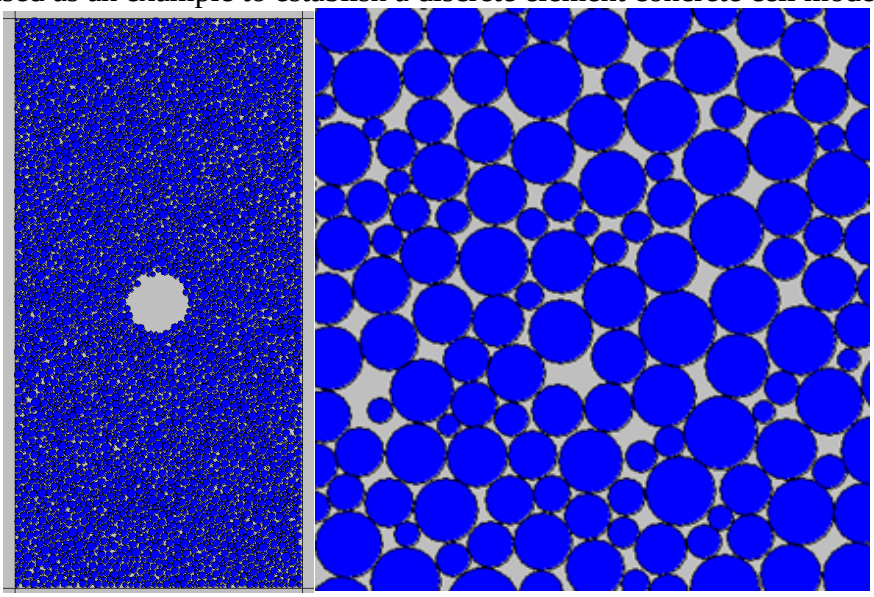

*Figure 3. Discrete element concrete particle flow simulation*

The corresponding elastic matrix can be obtained through two conditions, one is different velocity loads and boundary conditions which are applied to the unit cell, the other is the corresponding displacement field $\chi$. Finally, the compliance matrix of the orthotropic material can be converted according to elastic matrix.

$$C^H = E^{H^{-1}} = \begin{bmatrix} E_{11}^H & E_{12}^H & 0 \\ E_{21}^H & E_{22}^H & 0 \\ 0 & 0 & E_{33}^H \end{bmatrix}^{-1} = \begin{bmatrix} C_{11}^H & C_{12}^H & 0 \\ C_{21}^H & C_{22}^H & 0 \\ 0 & 0 & C_{33}^H \end{bmatrix}$$

The equivalent elastic coefficients $E_1, \nu_{21}$, $E_2$ and $\nu_{12}$ of concrete in the x and y directions like the equations below respectively:

$$E_1 = \frac{1}{C_{11}^H}, \nu_{21} = -\frac{C_{12}^H}{C_{22}^H}$$

$$E_2 = \frac{1}{C_{22}^H}, \nu_{12} = -\frac{C_{21}^H}{C_{11}^H}$$

By calculating and analyzing the unit cell model, the relationship can be obtained between the macroscopic equivalent elastic coefficient of concrete and the ratio of the unit cell size d to the maximum aggregate size $d_{max}$.

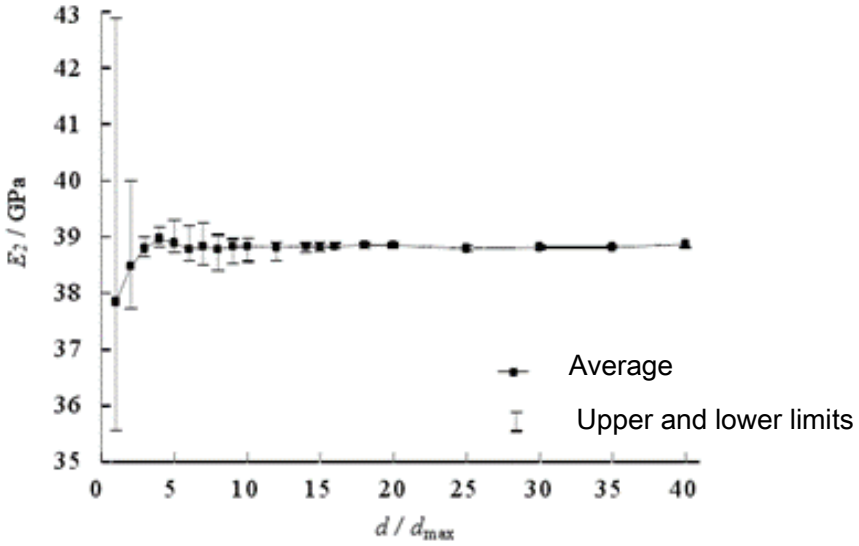


*Figure 4. Equivalent elastic modulus variation curve*

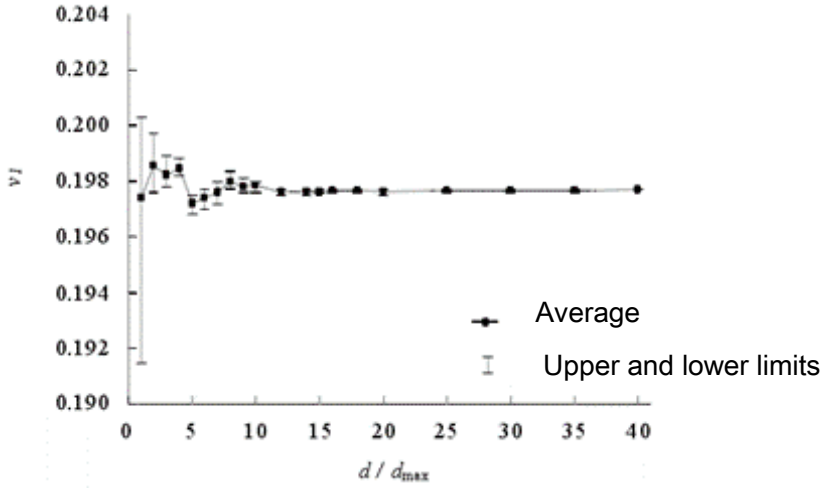


*Figure 5. Equivalent Poisson's ratio variation curve*

## 3. Comparative Analysis of Macro Finite Element

Based on the conclusion above, the side length of the concrete square unit cell is selected as d=4 and $d_{max}$=40mm, it is also essential to obtain the corresponding equivalent [11-17] elastic modulus and Poisson's ratio. Poisson's ratio are obtained. The macroscopic finite element mesh of ABAQUS software is used to numerically simulate the surface of the cable tower. At the same time, the macroscopic and mesoscopic multiscale models are used for simulation verification. The coarse grid size is 40 mm×40 mm, and the fine grid size is 1 mm×1 mm, as shown in the figure. Considering the slow calculation speed of finite element at the mesoscopic scale, the three-dimensional cable tower problem is converted into a two-dimensional planar problem, and the boundary conditions of the two-dimensional model are consistent with those of the three-dimensional model.

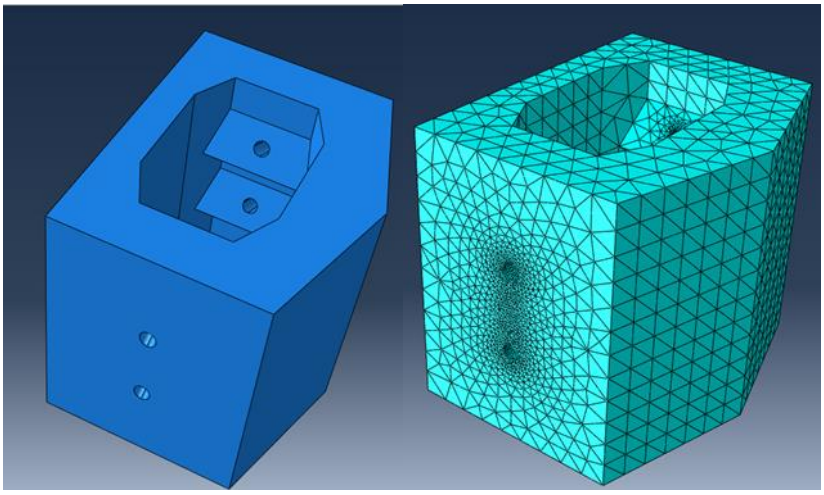

*Figure 6. Solid model of cable tower of Dachong Bridge*

This computational model considers the stress conditions of two segments under the maximum cable force. After calculation, a range of the same size on the surface of the cable tower is taken to study its macro- and micro-mechanical properties. The stress state and boundary conditions of the planar model are equivalent to those of the three-dimensional solid.

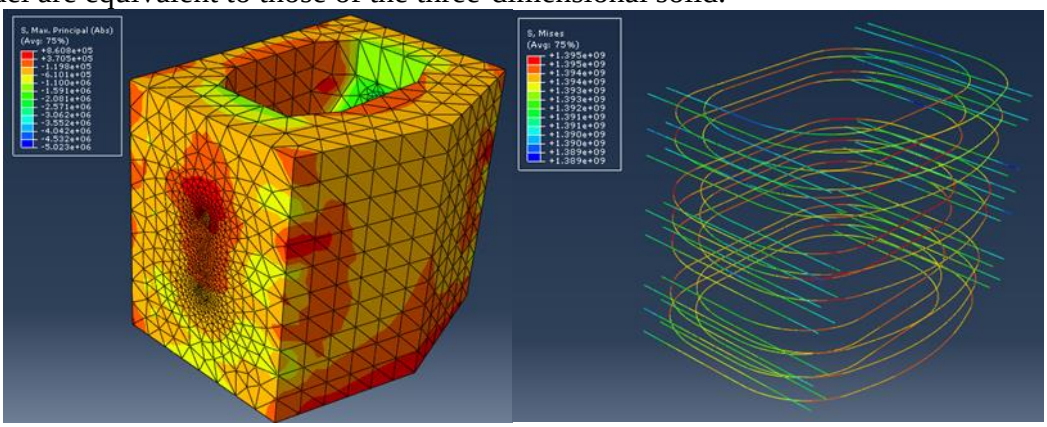

*Figure 7. Stress distribution and prestress loss of cable tower*

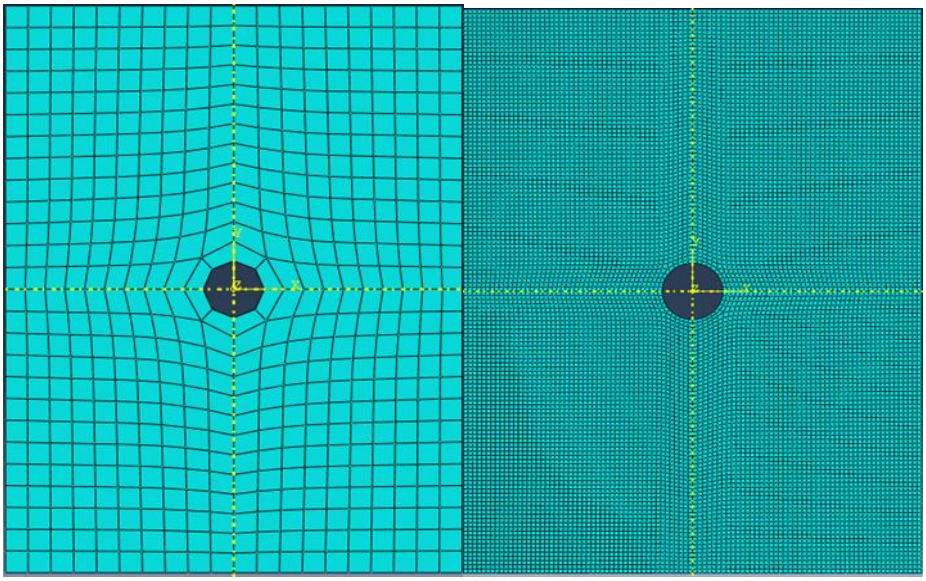

*Figure 8. Macro-micro and multi-scale model*

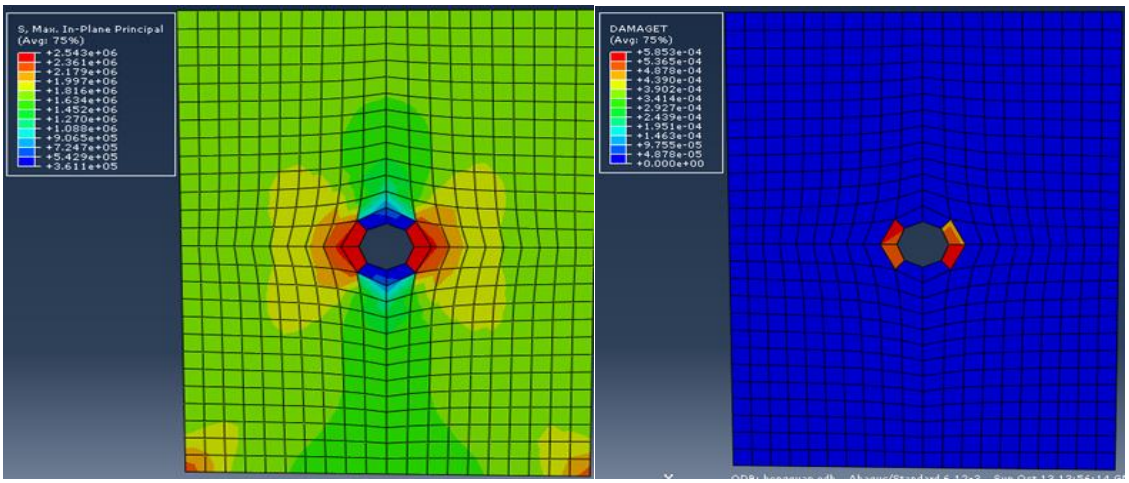


*Figure 9. macroscale calculation results (distribution of tensile stress and damage condition)*

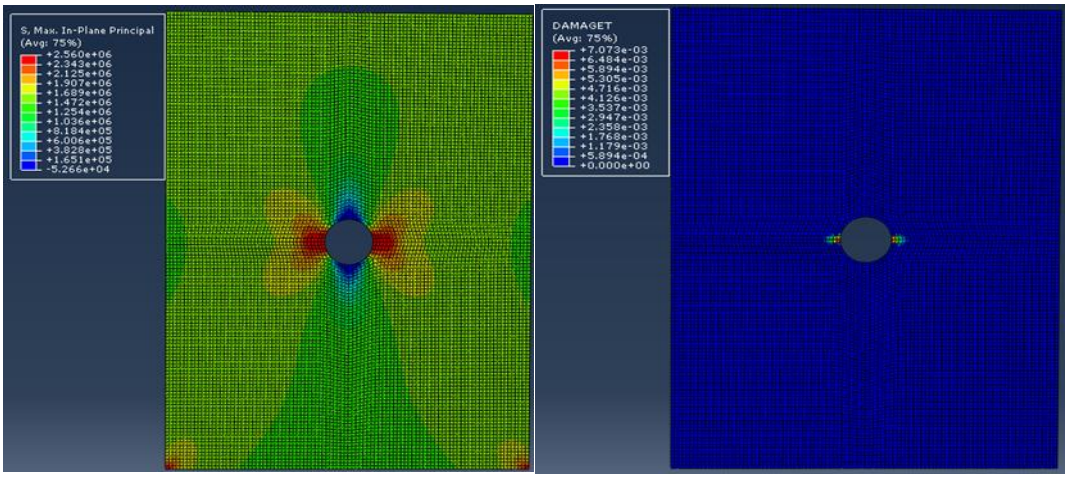


*Figure 10. Mesoscale calculation results (tensile stress distribution and damage condition)*

## 4. Conclusion

1. As $d/d_{max}$ increases, the phase differences between $E_1, v_{21}$, $E_2$ and $v_{12}$ gradually decrease. When $d/d_{max}$ is around 4-5, the error is minimal.

2. Comparing the macro- and micro-scale finite element calculation results of the cable tower surface, it can be seen that the distribution of both stresses and strains are basically the same, which indicates that the homogenization theory and finite element method can be used to better simulate the equivalent elastic coefficients of concrete.

## References


*[1] X.G. Li, J.T. Zhou, L.Y. Zhang, et al., Automatic monitoring of continuous rigid frame bridges by a magneto-elastic effffect method, International Journal of Robotics and Automation, 32(1), 2017, 41–47.*

*[2] J. Yang, J. Cheng, J.L. Wang, et al., Automatic deformation monitoring for large span bridge based on multi-constellation BDS and GPS system, International Journal of Robotics and Automation, 33(5), 2018, 534–541.*

*[3] J. Xin, H. Zhang, J. Zhou, et al., Damage identification of bridge system based on a hybrid algorithm, International Journal of Robotics and Automation, 34(2), 2019, 101–111.*

*[4] M. Li, Z. Sun, S. Liu, Y. Ma, H. Ma, C. Sun, and Y. Jia, Stereo vision technologies for China's lunar rover exploration mission, International Journal of Robotics and Automation, 31(2), 2016, 128–136.*

*[5] A.A. Dubov, Monitoring the stressed-strained state of pipelines, Tyazheloe Mashinostroenie, 11, 2004, 33–353.*

*[6] D.W. Yin, B.S. Xu, S.Y. Dong, et al., Characteristics of magnetic memory signals for medium carbon steel under static tensile conditions, Journal of Central South University, 12(s2), 2005, 107–111.*

*[7]Chinchane, A.; Sumant, O. Bridge Construction Market: Global Opportunity Analysis and Industry Forecst, 2020–2027; Allied Market*

*Research: Portland, OR, USA, 2020; p. 295.*

*[8] Leridon, H. World population outlook: Explosion or implosion. Popul. Soc. 2020, 573, 1–4.*

*[9] Morgese, M.; Ansari, F.; Domaneschi, M.; Cimellaro, G.P. Post-collapse analysis of Morandi's Polcevera viaduct in Genoa Italy. J.Civ. Struct. Health Monit. 2020, 10, 69–85.*

*[10]Cho, S.; Jo, H.; Jang, S.; Park, J.; Jung, H.-J.; Yun, C.-B.; Spencer Jr, B.F.; Seo, J.-W. Structural health monitoring of a cable-stayed*

*[11]bridge using wireless smart sensor technology: Data analyses. Smart Struct. Syst. 2010, 6, 461–480. [CrossRef]*

*[12] Nguyen, K.-D.; Kim, J.-T.; Park, Y.-H. Long-term vibration monitoring of cable-stayed bridge using wireless sensor network. Int.J. Distrib. Sens. Netw. 2013, 9, 804516.*

*[13]Park, J.C.; Shin, J.; Kim, H. Long-Term Monitoring of Seohae cable-stayed bridge using GNSS and SHMS. In Proceedings of the Instanbul Bridge Conference, Instanbul, Turkey, 11–13 August 2014.*

*[14]Marwala, T. Finite Element Model Updating Using Computational Intelligence Techniques: Applications to Structural Dynamics; Springer Science & Business Media: Berlin/Heidelberg, Germany, 2010.*

*[15]Sehgal, S.; Kumar, H. Structural dynamic model updating techniques: A state of the art review. Arch. Comput. Methods Eng. 2016,23, 515–533. [CrossRef]*

*[16]Alkayem, N.F.; Cao, M.; Zhang, Y.; Bayat, M.; Su, Z. Structural damage detection using finite element model updating with evolutionary algorithms: A survey. Neural Comput. Appl. 2018, 30, 389–411.*

*[17] Arjomandi, K.; Araki, Y.; MacDonald, T. Application of a hybrid structural health monitoring approach for condition assessment of cable-stayed bridges. J. Civ. Struct. Health Monit. 2019, 9, 217–231.*



Fucai Pei, working in Shandong Luqiao Group Co., Ltd, His main research interests include bridge construction control and health monitoring.



Ranran Hu graduated from Dalian University, Dalian, China in 2022 and she is currently studying in the field of road traffic at Shandong Jiaotong University.